

HCN IN CLOUD CORES: A GOOD TRACER OF CLASS 0 YOUNG STELLAR OBJECTS

JOÃO L. YUN AND MIGUEL C. MOREIRA

Observatório Astronómico de Lisboa, Tapada da Ajuda, P-1300 Lisboa, Portugal; yun@oal.ul.pt, miguelm@oal.ul.pt

JOSÉ M. AFONSO

Astrophysics Group, Imperial College of Science, Technology and Medicine, Prince Consort Road, London SW7 2BZ, UK; and Observatório Astronómico de Lisboa, Tapada da Ajuda, P-1300 Lisboa, Portugal; j.afonso@ic.ac.uk

AND

DAN P. CLEMENS

Institute for Astrophysical Research, Boston University, 725 Commonwealth Avenue, Boston, MA 02215; clemens@protostar.bu.edu

Received 1999 March 16; accepted 1999 April 15

ABSTRACT

We have conducted an HCN ($J = 1-0$) survey of 37 star-forming and quiescent dense cloud cores. HCN emission was detected toward 31 of the 33 cores containing embedded point sources, with only weak or no HCN detection among four starless sources. We find that the $J = 1-0$ transition of the HCN molecule is particularly well suited for revealing the early stages of star formation in molecular clouds. In the sample of star-forming cores, there is excellent spatial coincidence (better than $7''$) between the position of the peak integrated HCN emission and the location of the associated young stellar object (YSO). Furthermore, emission strength in this HCN transition is well correlated with the YSO class: Class 0 and Class I YSOs are preferentially detected. Detecting strong ($> 1 \text{ K km s}^{-1}$) HCN emission from a molecular cloud core indicates the presence of an embedded YSO and thus, indirectly, of a collapsing core. In addition, detection of very strong ($> 3 \text{ K km s}^{-1}$) HCN emission implies an 80% likelihood of the presence of an embedded Class 0 YSO.

Key words: ISM: clouds — ISM: molecules — stars: formation

1. INTRODUCTION

Star formation occurs in the densest regions of both giant molecular clouds and dark clouds. These clouds contain smaller and denser regions, the dense cores, with physical conditions adequate for the onset and later development of core collapse. The collapse of a core leads ultimately to the formation of a single star or a group of stars. Thus, knowing the physical conditions within cores is of crucial importance for our understanding of the details of this very early stage of star formation.

However, cold molecular hydrogen gas cannot in general be directly detected. In most cases, it has been traced using observations of other molecular transitions. The CO molecule is often used to trace relatively low density H_2 and can be used efficiently to delineate the extent of a molecular cloud. However, molecules with higher dipole moments are needed to search for dense cores within a cloud. For example, the $J = 1-0$ transition of the HCN molecule (dipole moment of 3 D) traces gas with densities $n \gtrsim 10^5 \text{ cm}^{-3}$ (e.g., Turner 1974), i.e., about 100 times denser than traced by the corresponding CO transition.

In a previous paper (Afonso, Yun, & Clemens 1998, hereafter AYC98), we have presented the results of an HCN ($J = 1-0$) survey of dense cores in a sample of 24 star-forming and quiescent Bok globules, the smallest and simplest molecular structures of the interstellar medium. The main goal was to study the physical properties of the dense cores and their relationships to the formation of the young stellar objects (YSOs) found embedded in the cores. We showed that HCN emission was detected toward 11 of 13 globules containing embedded point sources, with no HCN detection among 11 starless globules. Furthermore, we have shown that this HCN transition is well correlated with the YSO class, detecting preferentially Class I (and possibly

Class 0) YSOs. Our results indicated that detecting strong ($> 1 \text{ K km s}^{-1}$) HCN emission from a molecular cloud core seemed to imply the presence of an embedded protostar and thus, indirectly, of a collapsing core.

However, our globule sample contained no Class 0 sources. In order to test whether cloud cores containing Class 0 sources are also strong HCN emitters (which has consequences for the picture of the precollapse evolution of a dense core), we needed to determine the intensity level of HCN emission in Class 0 objects. In this paper, we report observations toward a new sample of cloud cores, many of which contain YSOs in different stages of evolution, and many of which contain Class 0 objects.

By searching for HCN emission from a sample of clouds containing quiescent and star-forming examples, i.e., containing starless clouds and clouds with YSOs, we seek to probe the physical conditions of the evolutionary stages of a molecular cloud core during the star formation process. In so doing, we are able to estimate the duration of detectable HCN emission, and we link this emission to the presence of protostellar sources embedded in the cloud cores.

In this paper, we present our HCN survey of molecular gas associated with YSOs at different stages of evolution. Applications of these results to studies of the star formation process are discussed. In § 2, we describe the observations and data reduction. In § 3, we present and discuss our results, and in § 4 we summarize our findings.

2. OBSERVATIONS AND DATA REDUCTION

The sample of Bok globules surveyed for HCN and described in AYC98 did not contain Class 0 sources. Therefore, the new sample of cloud cores was selected mainly by the requisite of their being associated with Class 0 sources. No distinction has been made as to the type of star forma-

tion environment (small globules and dark cloud cores accepted indiscriminately). Furthermore, for the purposes of comparison and statistics, a few cores associated with non-Class 0 sources (starless or associated with Class I, Class II, or small clusters of YSOs) were added to the new sample presented in Table 1. Most of the sources were extracted from tables of Class 0 sources contained in Gregersen et al. (1997) and Yun et al. (1996). In both cases the tables are a compilation from the literature.

Millimeter observations at 88.63 GHz (the $J = 1-0$ rotational transition of HCN) were carried out toward this sample of YSOs using the 15 m Swedish-ESO Submillimetre Telescope of the European Southern Observatory during 1998 September 22–24. The half-power beamwidth of the telescope was $56''$ at the observing frequency. The main-beam efficiency was 0.75. The back end

included a 1000-channel acousto-optical spectrometer with 43 kHz resolution (0.15 km s^{-1}). Each source was observed using dual beam switching (chop throw of $11'$) with integration times of 4 minutes toward each position. The pointing error was found to be better than $7''$. We obtained a five-point map for each source, taken in an approximately full-beam-spaced grid.

Spectral line intensities were calibrated and corrected for atmospheric losses using the standard chopper-wheel method to obtain the antenna temperature, T_A^* . The data were processed using standard procedures of the Continuum and Line Analysis Single-dish Software (CLASS) package developed at Observatoire de Grenoble and IRAM. Baselines were fitted and removed, followed by Gaussian fitting, yielding the values of the line parameters (peak, width, and integrated intensity).

TABLE 1
HCN SURVEY OF DENSE CORES

Source Name (1)	R.A. (B1950.0) (2)	Decl. (B1950.0) (3)	Associated Point Source (4)	V_{LSR} (km s^{-1}) (5)	Δv_{FWHM} (km s^{-1}) (6)	$T_{\text{R}}^{F=2-1}$ (K) (7)	$I_{\text{HCN}}^{F=2-1}$ (K km s^{-1}) (8)	T_{R} (K) (9)	I_{HCN} (K km s^{-1}) (10)
T Tauri	04 19 04.2	19 25 06	II ^a	8.30	1.3 (0.1)	0.68 (0.06)	0.94 (0.04)	1.02 (0.11)	1.36 (0.08)
L1551 NE ^b	04 28 50.5	18 02 10	0	7.44	...	>0.58	>1.73	>1.18	>3.26
L1527	04 38 48.0	25 57 05	0	<0.11	<0.16	<0.11	<0.16
RNO 43 MM	05 29 30.6	12 47 35	0	9.97	1.51 (0.07)	0.65 (0.06)	1.04 (0.04)	1.59 (0.12)	2.12 (0.08)
NGC 2024 FIR 5	05 39 13.0	-01 57 08	0	10.93	2.18 (0.14)	7.91 (0.09)	18.32 (0.27)	13.65 (0.27)	34.08 (0.81)
HH 24 MMS	05 43 35.1	-00 11 47	0	9.84	1.48 (0.02)	2.41 (0.06)	3.80 (0.06)	4.60 (0.18)	7.03 (0.18)
CB 35	05 44 27.0	10 25 33	Starless	<0.10	<0.15	<0.10	<0.15
NGC 2264G	06 38 25.7	09 58 55	0	4.28	1.49 (0.24)	0.20 (0.04)	0.31 (0.03)	0.65 (0.12)	0.77 (0.08)
IRAS 08124–3422	08 12 29.6	-34 22 02	0	4.64	1.07 (0.02)	1.30 (0.05)	1.48 (0.03)	2.40 (0.15)	2.61 (0.09)
IRAS 08261–5100	08 26 11.6	-51 00 39	I	5.33	1.51 (0.14)	0.24 (0.05)	0.38 (0.01)	0.49 (0.15)	0.80 (0.03)
IRAS 08337–4028	08 33 42.6	-40 28 02	^c	7.10	2.97 (0.14)	1.80 (0.06)	5.69 (0.07)	3.12 (0.18)	10.36 (0.21)
IRAS 11590–6452	11 59 03.1	-64 52 11	0	-4.80	1.31 (0.03)	3.85 (0.11)	5.39 (0.08)	7.63 (0.33)	10.25 (0.24)
IRAS 12345–6911	12 34 46.5	-69 11 06	II	<0.11	<0.17	<0.11	<0.17
IRAS 13036–7644 ^b	13 03 41.0	-76 44 03	0	3.86	...	>0.95	>2.19	>1.90	>4.60
IRAS 13224–5928	13 22 30.0	-59 28 15	II	-33.12	1.33 (0.07)	0.38 (0.03)	0.54 (0.02)	0.80 (0.09)	1.09 (0.06)
Sz 83	15 53 24.4	-37 40 35	II	4.92	1.29 (0.16)	0.24 (0.06)	0.33 (0.04)	0.43 (0.11)	0.47 (0.06)
IRAS 16029–4548	16 02 57.0	-45 48 08	II	<0.11	<0.16	<0.11	<0.16
VLA 1623	16 23 24.9	-24 17 46	0	2.18	1.10 (0.04)	1.11 (0.07)	1.30 (0.04)	2.15 (0.21)	3.33 (0.15)
V346 Nor	16 28 57.0	-44 49 06	^d	-3.18	1.55 (0.05)	1.33 (0.07)	2.21 (0.05)	2.65 (0.21)	4.20 (0.15)
IRAS 16293–2422 ^b	16 29 20.9	-24 22 13	0	3.69	...	>2.40	>6.83	>4.46	>13.65
IRAS 17012–3603	17 01 12.0	-36 03 10	0	10.57	1.37 (0.09)	0.40 (0.06)	0.57 (0.04)	0.80 (0.18)	1.05 (0.09)
IRAS 17157–3215	17 15 44.0	-32 15 36	I	10.92	1.68 (0.01)	0.40 (0.06)	0.71 (0.04)	0.76 (0.18)	1.96 (0.17)
IRAS 17159–3324	17 15 55.0	-33 24 16	I	7.48	1.56 (0.11)	0.41 (0.07)	0.68 (0.04)	0.84 (0.21)	1.35 (0.13)
IRAS 17172–4316	17 17 15.9	-43 16 54	I	-7.41	1.22 (0.03)	0.81 (0.04)	1.07 (0.03)	1.48 (0.12)	1.99 (0.07)
IRAS 17181–4405	17 18 09.3	-44 05 48	^e	-13.04	2.10 (0.06)	0.83 (0.06)	1.84 (0.04)	1.45 (0.18)	3.43 (0.14)
IRAS 17193–4319	17 19 18.0	-43 19 24	0	-8.88	1.94 (0.02)	2.76 (0.07)	5.68 (0.05)	5.24 (0.21)	10.65 (0.15)
CB 98	17 44 02.0	-20 29 26	^f	10.35	0.60 (0.04)	0.92 (0.07)	0.59 (0.03)	2.01 (0.21)	1.24 (0.08)
BHR 145	17 44 23.0	-43 42 12	Starless	7.75	0.92 (0.15)	0.19 (0.07)	0.17 (0.03)	0.49 (0.21)	0.48 (0.09)
BHR 142	17 59 18.0	-46 39 54	Starless	5.67	1.02 (0.11)	0.24 (0.06)	0.25 (0.03)	0.61 (0.18)	0.65 (0.09)
CB 112	18 06 00.0	-01 50 33	Starless	<0.11	<0.17	<0.11	<0.17
CB 130	18 13 38.0	-02 33 52	^f	7.66	1.67 (0.55)	0.11 (0.07)	0.19 (0.05)	0.83 (0.21)	0.84 (0.10)
L483 ^b	18 14 50.6	-04 40 49	0	5.11	...	>0.67	>1.57	>1.95	>3.39
IRAS 18162–2048	18 16 13.0	-20 48 49	0	12.81	3.28 (0.12)	0.59 (0.06)	2.05 (0.07)	1.13 (0.18)	3.55 (0.17)
Serpens SMM 1 ^b	18 27 17.3	01 13 23	0	8.51	...	>2.01	>7.50	>2.79	>7.73
Serpens SMM 2	18 27 28.0	01 10 45	0	7.08	1.96 (0.02)	3.23 (0.07)	6.73 (0.06)	5.81 (0.21)	14.00 (0.20)
L723	19 15 42.0	19 06 55	0	10.72	2.12 (0.17)	0.34 (0.06)	0.77 (0.06)	0.81 (0.17)	1.88 (0.16)
B335	19 34 35.7	07 27 15	0	8.22	...	>0.80	>0.80	>1.81	>1.84

NOTES.—Units of right ascension are hours, minutes, and seconds, and units of declination are degrees, arcminutes, and arcseconds. Errors are 1σ and upper limits are 2σ .

^a There could be some contribution from the younger, more embedded, infrared companion.

^b Spectrum exhibits strong self-absorption.

^c Embedded cluster (Santos et al. 1998).

^d FU Orionis star (with a possible younger, more embedded, infrared companion; Reipurth et al. 1997).

^e Several embedded sources (Santos et al. 1998).

^f Weak millimeter source (Launhardt & Henning 1997).

3. RESULTS AND DISCUSSION

In Table 1 we list the sources observed. Columns (2) and (3) give the positions observed toward each source. When available, we give in column (4) the associated YSO class, according to the classification of Adams, Lada, & Shu (1987), extended by André, Ward-Thompson, & Barsony (1993). Columns (5)–(10) give the results of the HCN survey. Columns (5)–(8) list, respectively, the line velocity V_{LSR} , the FWHM line width Δv , the line peak T_R (antenna temperature corrected for the main-beam efficiency), and the integrated line intensity (area, $I_{\text{HCN}} = \int T_R dv$) for the central line component ($F = 2-1$ transition, usually the most intense). Columns (9) and (10) give respectively the line peak and the integrated line intensity of the three hyperfine components summed together. Values in parentheses are 1σ

errors, and upper limits are 2σ . For nondetections, the upper limit in the integrated emission, σ_I , is the area of a Gaussian line with peak intensity equal to σ_{T_R} and FWHM equal to the largest Δv_{FWHM} among the weakest detections.

3.1. Spectra and Maps

In Figures 1 and 2 we present two examples of the spectra obtained. The first example (Fig. 1) shows the spectra of RNO 43 MM, in which the hyperfine structure of the $J = 1-0$ rotational transition of the HCN molecule is clearly seen. The main line splits into three components: $F = 0-1$ (88633.9 MHz), $F = 2-1$ (88631.8 MHz), and $F = 1-1$ (88630.4 MHz) (see, e.g., De Lucia & Gordi 1969; Bogey, Demuynck, & Destombes 1981). The second example (Fig. 2) reveals self-absorbed spectra of IRAS

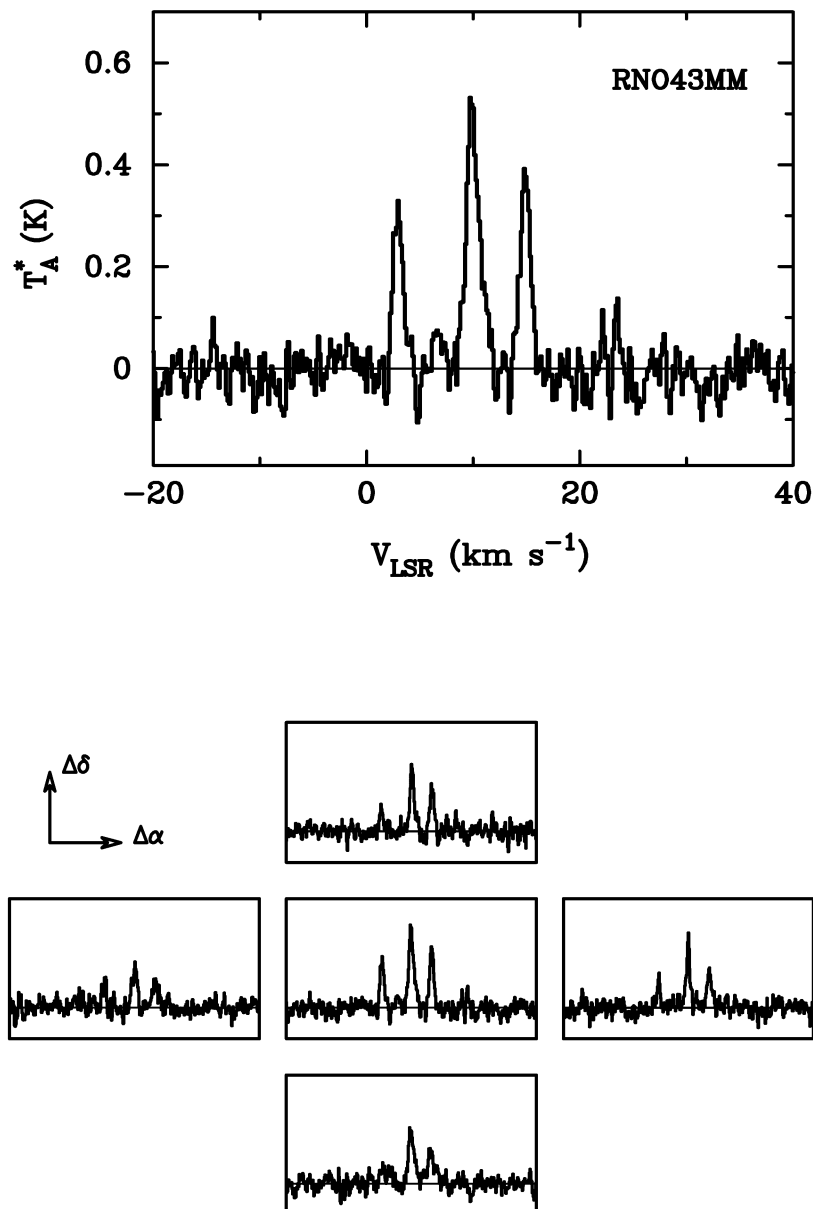


FIG. 1.—*Top*: Example of spectra obtained toward RNO 43 MM. The hyperfine splitting of the $J = 1-0$ rotational line of HCN is clearly seen. *Bottom*: Map of HCN emission-line profiles for RNO 43 MM. The spectra are presented in their relative angular positions. The horizontal velocity axis and the vertical antenna temperature axis are the same as in the top panel.

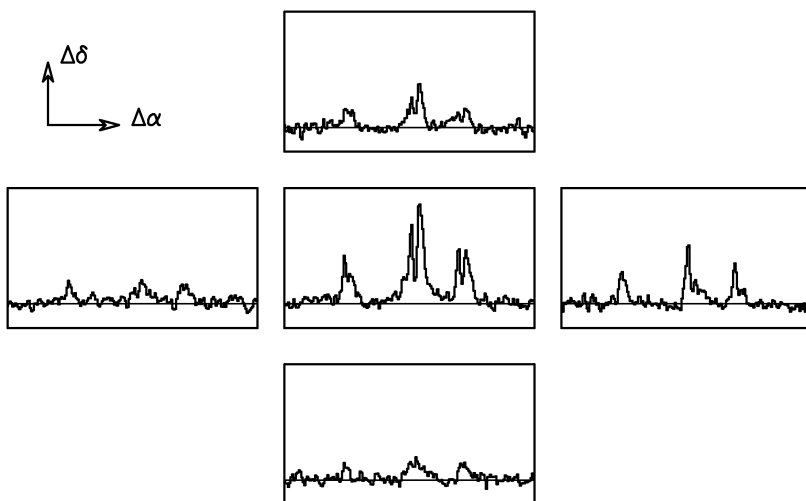
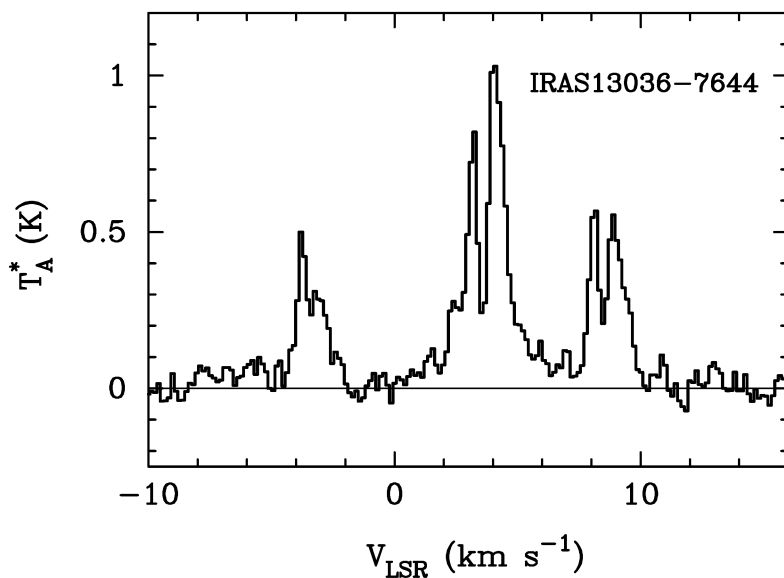


FIG. 2.—*Top*: Example of self-absorbed spectra obtained toward IRAS 13036–7644. The hyperfine splitting of the $J = 1-0$ rotational line of HCN is clearly seen. *Bottom*: Map of HCN emission-line profiles for IRAS 13036–7644. The spectra are presented in their relative angular positions. The horizontal velocity axis and the vertical antenna temperature axis are the same as in the top panel.

13036–7644, indicating the presence of very large optical depths. Self-absorbed lines were also seen toward L1551 NE, IRAS 16293–2422, L483, and Ser SMM 1.

Figures 1 and 2 also reveal that the HCN emission tends to peak at the position of the YSO (located at the center of the five-point map). This good spatial coincidence between the peaks of the HCN emissions and the location of the associated YSOs reinforces our previous finding (AYC98) that the HCN emission is related to the presence of the YSOs in the cores.

3.2. HCN, *Starless Clouds*, and the Evolutionary Stages of YSOs

Analysis of Table 1 indicates that the strongest HCN emission was detected toward sources with associated Class 0 YSOs. In order to better visualize this trend, for the

objects with an entry in column (4), we have plotted, in Figure 3, the total HCN integrated line intensity given in column (10) of Table 1 versus the class of the associated YSO (given in col. [4]). Each circle and horizontal line in Figure 3 corresponds to one source and its associated YSO. The sources without a known associated embedded YSO appear in the class of “starless” clouds. Arrows represent upper and lower limits.

From left to right and from top to bottom, the sources represented in this figure are as follows:

Starless.—BHR 142, BHR 145, CB 112, CB 35;

Class 0.—NGC 2024 FIR 5, Ser SMM 2, IRAS 16293–2422, IRAS 17193–4319, IRAS 11590–6452, Ser SMM 1, HH 24 MMS, IRAS 13036–7644, IRAS 18162–2048, L483, VLA 1623, L1551 NE, IRAS

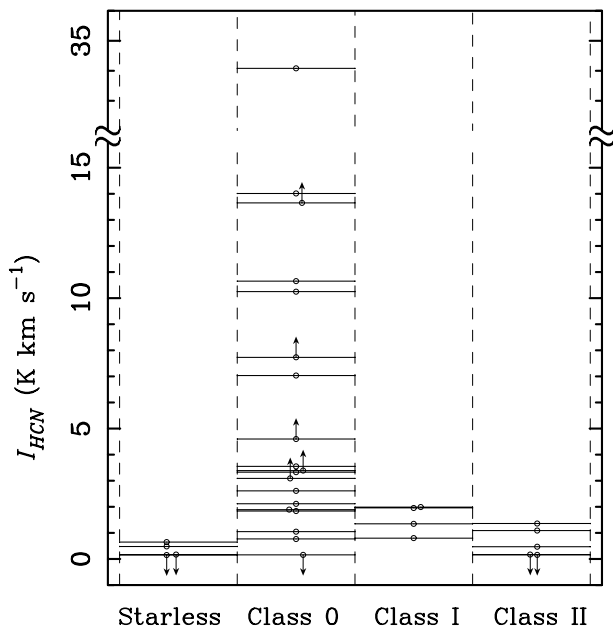


FIG. 3.—HCN emission and the presence (or absence) of a point source. All very strong emissions were detected toward cores with an associated Class 0 YSO. See § 3.2 for a description.

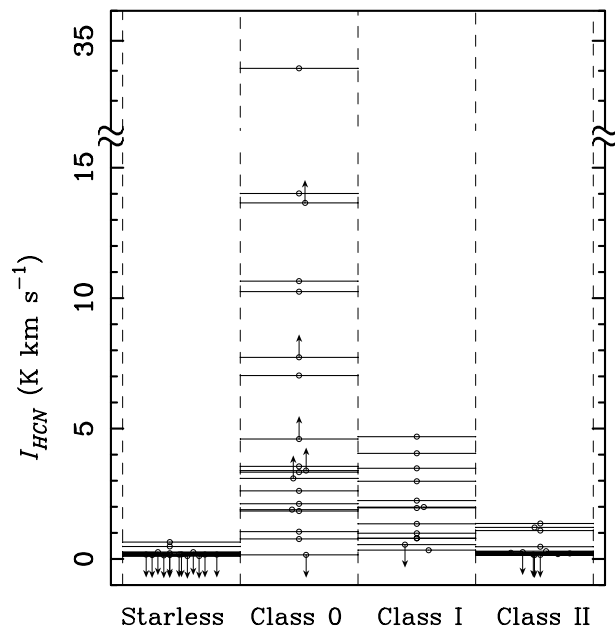


FIG. 4.—Same as Fig. 3, but including the sources from AYC98

08124–3422, RNO 43 MM, L723, B335, IRAS 17012–3603, NGC 2264G, L1527;

Class I.—IRAS 17172–4316, IRAS 17157–3215, IRAS 17159–3324, IRAS 08261–5100;

Class II: T Tauri, IRAS 13224–5928, Sz 83, IRAS 12345–6911, IRAS 16029–4548.

Figure 3 shows that only weak HCN detection ($I_{\text{HCN}} < 1 \text{ K km s}^{-1}$) occurred for the starless clouds. In addition, the highest values of HCN emission are seen only toward the sources with associated Class 0 YSOs.

For a more complete analysis of the relationship between HCN emission and the evolutionary stage of a cloud core, we present in Figure 4 the same information as in Figure 3 but including the sources from AYC98. A breakdown of the HCN brightness of the sources included in Figure 4 is shown in Table 2. The group of sources with associated Class 0 YSOs appears as a distinct group when we consider the presence of very strong HCN emission (defined here as $I_{\text{HCN}} > 3 \text{ K km s}^{-1}$). In this group, more than half (12/19) of the sources exhibit very strong HCN emission, while only 8% (3/40) of the sources without an associated Class 0 YSO show very strong HCN emission. From these numbers, we estimate that detection of very strong HCN emission implies an 80% likelihood of having found an embedded Class 0 YSO.

Figure 5 shows the cumulative fraction of sources with integrated intensities smaller than or equal to a fixed value.

The rightmost curve corresponds to the group of sources with an associated Class 0 YSO; the curve to the left corresponds to the group without an associated Class 0 YSO. About 60% of the sources in the former group show very strong HCN emission, whereas this is true for only 8% of sources in the latter group. The probability that the values of I_{HCN} observed for the two data sets (the Class 0 group

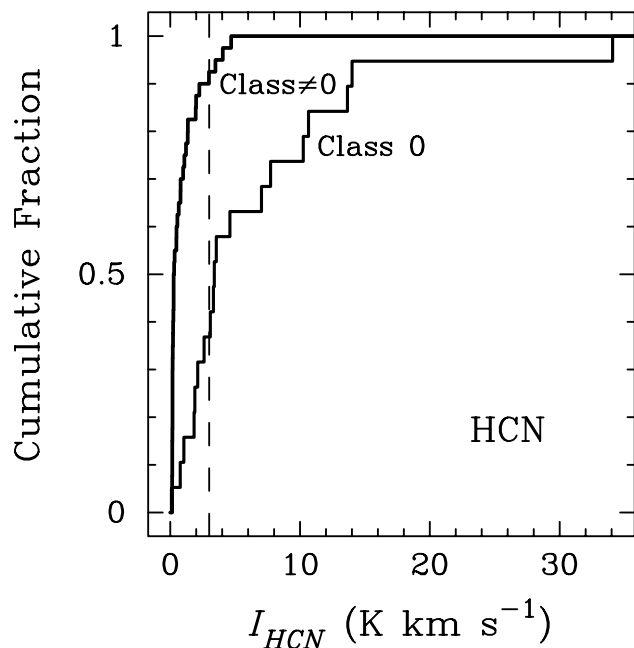


FIG. 5.—Cumulative fraction of sources with HCN integrated intensity smaller than or equal to a fixed value. The line to the right shows the sources with associated Class 0 objects; the line to the left shows the starless sources or those with non-Class 0 objects. Note the large number of sources with large I_{HCN} values in the Class 0 group sources. The dashed vertical line is drawn at $I_{\text{HCN}} = 3 \text{ K km s}^{-1}$. About 60% of the Class 0 group sources have $I_{\text{HCN}} > 3 \text{ K km s}^{-1}$, while this is the case for only less than 10% of the non-Class 0 group sources.

TABLE 2

BREAKDOWN OF THE SOURCES SURVEYED: HCN INTENSITY AND CLASS 0 SOURCES

Type	$I_{\text{HCN}} > 3$	$I_{\text{HCN}} < 3$	Total
Class 0	12	7	19
Non-Class 0	3	37	40
Total	15	44	59

and the non-Class 0 group) come from a single parent distribution is 0.002% (Kolmogorov-Smirnov test).

The absence of, or very low emission values for, HCN emission in the group of starless cores indicates that the stage of the star formation process between when the cloud core becomes sufficiently dense to excite the HCN $J = 1-0$ transition and the appearance of an infrared point source is very brief. If the horizontal axis in Figure 4 is seen as a temporal axis, the concentration of strong HCN detections seen in this figure indicates that HCN emission is a relatively transient phenomenon and that strong emission occurs only during the period of protostellar accretion. As described in AYC98, this is in good agreement with estimates of the timescale for the formation of a dense core and the timescale for protostellar accretion (e.g., Fiedler & Mouschovias 1993). It appears that once a cloud core reaches a sufficiently high density, enabling both HCN excitation and the start of protostellar accretion, it will rapidly form a YSO (first detected as a Class I or Class 0 source). As a result, we expect that it should be very difficult to detect a core with strong HCN emission and no YSO.

3.3. HCN, Ammonia, and CS

Since the work of Myers & Benson (1983), ammonia has been used to identify dense cores in dark clouds. In addition, in the past few years, CS has also been used to trace dense material within molecular clouds. However, until now neither of these two tracers has been shown to be useful in establishing an observational distinction between starless and star-forming cores.

Myers et al. (1987) have found that about half of the ammonia-traced dense cores were associated with *IRAS* sources, while the other half were starless. Lemme et al. (1996), in their survey of ammonia in Bok globules, found a large number of starless globules exhibiting strong NH_3 (1, 1) emission.

Using data from Matthews & Little (1983), Torrelles et al. (1986), Bourke et al. (1995), Anglada et al. (1996), Lemme et al. (1996), and Anglada, Sepúlveda, & Gómez (1997), we have assembled the integrated line intensity of the ammonia (1, 1) transition for 48 of the sources included in Figure 4. The 11 remaining sources do not have ammonia data in the literature.

We plot the ammonia integrated line intensities in Figures 6 and 7, which are the same as Figures 4 and 5, respectively, but for ammonia instead of HCN. As in the case of HCN, ammonia emission is stronger toward sources with associated Class 0 and Class I YSOs than it is for the remaining cases. However, a comparison of Figures 5 and 7 indicates that the separation of starless and Class 0/I sources is more enhanced for HCN than it is for ammonia. The corresponding Kolmogorov-Smirnov test gives a match probability of 0.04%, 20 times higher than the HCN value.

The comparison described in the previous paragraph should in fact be done with the same sample of sources for both HCN and ammonia. Therefore, we have repeated the comparison excluding from the HCN sample the same 11 sources that do not have ammonia data. No significant deviation was found from the results described above.

The fraction of starless cores among strong ammonia detections is much higher than among starless HCN cores. We thus confirm that while ammonia traces dense cores, HCN is more selective at detecting cores with embedded

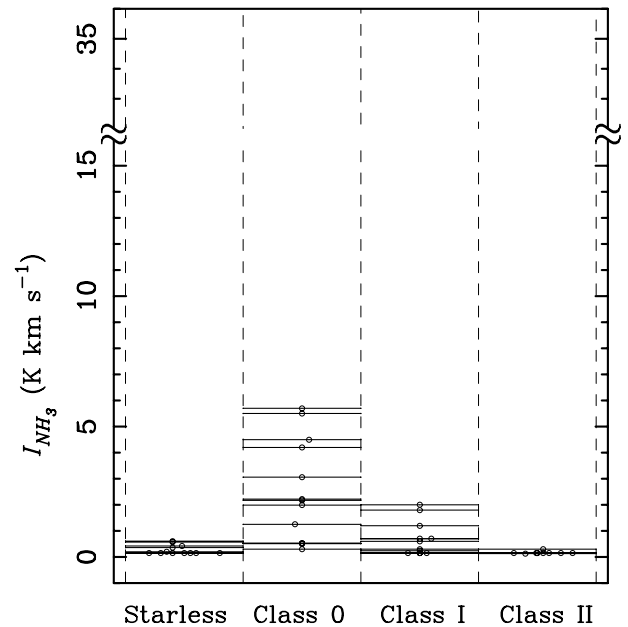


FIG. 6.—Same as Fig. 4, but for ammonia emission instead of HCN

objects. In particular, very strong ($> 3 \text{ K km s}^{-1}$) HCN emission is a useful tool for locating Class 0 objects.

According to the chemical evolutionary models of Scappini et al. (1998), in the initial stages of the evolution of a diffuse cloud to form a dense cloud core, the abundance of HCN is about 3 orders of magnitude higher than that of ammonia. However, the relatively low density of those initial stages ($\leq 10^4 \text{ cm}^{-3}$) and the high value of the HCN critical density ($\geq 10^5 \text{ cm}^{-3}$) should suppress any HCN emission during this low-density period. At a later stage, but still before a point source has been formed in the cloud core,

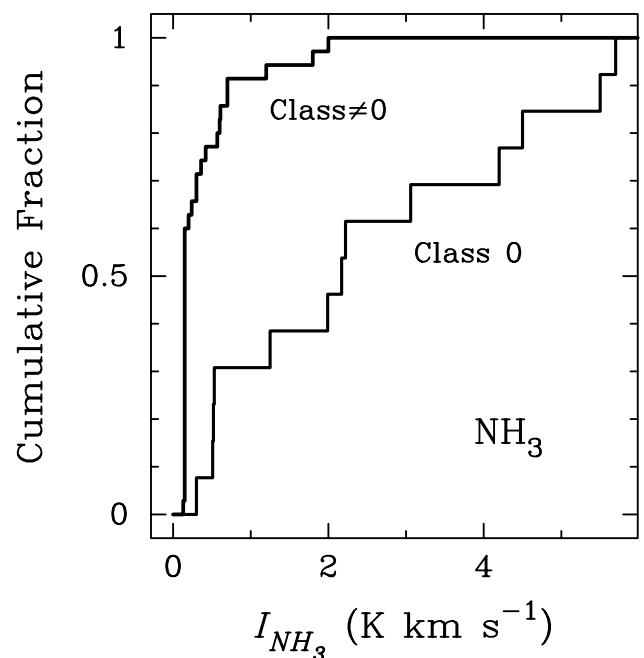


FIG. 7.—Same as Fig. 5, but for ammonia emission instead of HCN

the abundance of ammonia rises sharply, becoming 2–3 orders of magnitude higher than that of HCN, favoring a stronger ammonia emission from a still starless core. The buildup of the HCN abundance is more gradual, and large HCN abundances are obtained later, very likely when the density has reached the value required to excite the HCN $J = 1-0$ rotational transition.

A similar analysis is needed for the CS transitions in order to investigate whether CS transitions can distinguish between starless cores and star-forming cores.

4. SUMMARY

We have conducted HCN ($J = 1-0$) observations of a sample of YSOs. Of the 37 sources, four were starless (with no evidence for embedded YSOs), 19 were associated with Class 0 YSOs, four were associated with Class I YSOs, and five were associated with Class II YSOs. The remaining five sources represent cores that could not be classified with certainty.

1. HCN emission was detected toward 31 sources: two starless (weak), 18 Class 0 YSOs (mostly very strong), four Class I YSOs (strong), and three Class II YSOs (weak). The remaining five unclassified sources were also positive detections.

2. Very strong ($>3 \text{ K km s}^{-1}$) HCN emission is seen toward 12 (of 19) cores lodging embedded Class 0 YSOs.

Strong ($>1 \text{ K km s}^{-1}$) HCN emission is seen toward most Class I sources and from two Class II YSOs.

3. The spatial distribution of the HCN emission tends to peak at the position of the associated YSO point source.

4. The $J = 1-0$ transition of the HCN molecule detects preferentially Class 0 and Class I YSOs.

5. The strong presence of the $J = 1-0$ transition of the HCN molecule signifies recent star formation in small molecular clouds. Detecting strong ($>1 \text{ K km s}^{-1}$) HCN emission seems to imply the presence of a collapsing core.

6. Class 0 sources are embedded within dense cores that are very strong HCN emitters. Detecting very strong ($>3 \text{ K km s}^{-1}$) HCN emission indicates an 80% likelihood of having found an embedded Class 0 YSO.

7. The physical conditions required to excite strong HCN ($J = 1-0$) emission are either reached by the time a protostellar core has formed (at about the end of the ambipolar diffusion stage or beginning of the protostellar accretion stage) or are coeval with protostar formation.

This work has been partially supported by a Fundação para a Ciência e Tecnologia (FCT) grant to J. L. Y. and by NASA grant NAG 5-3337 to D. P. C. Support from FCT to M. C. M. and from Fundação Gulberrkian to J. M. A. in the form of scholarships is gratefully acknowledged.

REFERENCES

- Adams, F. C., Lada, C. J., & Shu, F. H. 1987, *ApJ*, 312, 788
 Afonso, J. M., Yun, J. L., & Clemens, D. P. 1998, *AJ*, 115, 1111 (AYC98)
 André, P., Ward-Thompson, D., & Barsony, M. 1993, *ApJ*, 406, 122
 Anglada, G., Estalella, R., Pastor, J., Rodríguez, L. F., & Haschick, A. D. 1996, *ApJ*, 463, 205
 Anglada, G., Sepúlveda, I., & Gómez, J. F. 1997, *A&AS*, 121, 255
 Bogey, M., Demuynck, C., & Destombes, J.-L. 1981, *Mol. Phys.*, 43, 1043
 Bourke, T. L., Hyland, A. R., Robinson, G., James, S. D., & Wright, C. M. 1995, *MNRAS*, 276, 1067
 De Lucia, F., & Gordi, W. 1969, *Phys. Rev.*, 187, 58
 Fiedler, R. A., & Mouschovias, T. C. 1993, *ApJ*, 415, 680
 Gregersen, E. M., Evans, N. J., Zhou, S., & Choi, M. 1997, *ApJ*, 484, 256
 Launhardt, R., & Henning, T. 1997, *A&A*, 326, 329
 Lemme, C., Wilson, T. L., Tieftrunk, A. R., & Henkel, C. 1996, *A&A*, 312, 585
 Matthews, N., & Little, L. T. 1983, *MNRAS*, 205, 123
 Myers, P. C., & Benson, P. J. 1983, *ApJ*, 266, 309
 Myers, P. C., Fuller, G. A., Mathieu, R. D., Beichman, C. A., Benson, P. J., Schild, R. E., & Emerson, J. P. 1987, *ApJ*, 319, 340
 Reipurth, B., Olberg, M., Gredel, R., & Booth, R. S. 1997, *A&A*, 327, 1164
 Santos, N. C., Yun, J. L., Santos, C. A., & Marreiros, R. G. 1998, *AJ*, 116, 1376
 Scappini, F., Cecchi-Pestellini, C., Olberg, M., Casalori, A., & Fanti, C. 1998, *ApJ*, 504, 866
 Torrelles, J. M., Ho, P. T. P., Moran, J. M., Rodríguez, L. F., & Cantó, J. 1986, *ApJ*, 307, 787
 Turner, B. E. 1974, in *Galactic and Extra-Galactic Radio Astronomy*, ed. G. L. Verschuur & K. I. Kellermann (New York: Springer), 199
 Yun, J. L., Moreira, M. C., Torrelles, J. M., Afonso, J. M., & Santos, N. C. 1996, *AJ*, 111, 841